Time-resolved photoluminescence study of CdSe/CdMnS/CdS core/multi-shell nanoplatelets

J. R. Murphy, S. Delikanli, T. Scrace, P. Zhang, T. Norden, T. Thomay, A. N. Cartwright, H. V. Demir, and A. Petrou

Citation: Appl. Phys. Lett. **108**, 242406 (2016); doi: 10.1063/1.4953840
View online: https://doi.org/10.1063/1.4953840
View Table of Contents: http://aip.scitation.org/toc/apl/108/24
Published by the American Institute of Physics

Time-resolved photoluminescence study of CdSe/CdMnS/CdS core/multi-shell nanoplatelets

J. R. Murphy,[1,2] S. Delikanli,[3,4] T. Scrace,[2] P. Zhang,[2] T. Norden,[2] T. Thomay,[1] A. N. Cartwright,[1] H. V. Demir,[3,4,a)] and A. Petrou[2,b)]
[1]*Department of Electrical Engineering, State University of New York, University at Buffalo, Buffalo, New York 14260, USA*
[2]*Department of Physics, State University of New York, University at Buffalo, Buffalo, New York 14260, USA*
[3]*LUMINOUS! Center of Excellence for Semiconductor Lighting and Displays, School of Electrical and Electronic Engineering, School of Physical and Materials Sciences, Nanyang Technological University, Singapore 639798*
[4]*Department of Electrical and Electronics Engineering, Department of Physics, UNAM—Institute of Materials Science and Nanotechnology, Bilkent University, Ankara 06800, Turkey*

(Received 8 April 2016; accepted 26 May 2016; published online 13 June 2016)

We used photoluminescence spectroscopy to resolve two emission features in CdSe/CdMnS/CdS and CdSe/CdS core/multi-shell nanoplatelet heterostructures. The photoluminescence from the magnetic sample has a positive circular polarization with a maximum centered at the position of the lower energy feature. The higher energy feature has a corresponding signature in the absorption spectrum; this is not the case for the low-energy feature. We have also studied the temporal evolution of these features using a pulsed-excitation/time-resolved photoluminescence technique to investigate their corresponding recombination channels. A model was used to analyze the temporal dynamics of the photoluminescence which yielded two distinct timescales associated with these recombination channels. The above results indicate that the low-energy feature is associated with recombination of electrons with holes localized at the core/shell interfaces; the high-energy feature, on the other hand, is excitonic in nature with the holes confined within the CdSe cores. *Published by AIP Publishing*. [http://dx.doi.org/10.1063/1.4953840]

Recently, colloidal semiconductor nanoplatelets (NPL) have attracted considerable attention.[1–8] These are quasi two-dimensional structures grown using relatively inexpensive solution-based synthesis methods, which have a significant cost advantage when compared to molecular beam epitaxy (MBE) and chemical vapor deposition (CVD) growth techniques. In addition, nanoplatelets also offer the following advantages: (a) a tunable emission spectrum, which is narrower than that of colloidal quantum dots (cQDs)[7,9] and (b) an enhanced absorption cross-section.[10]

Our previous study of CdSe/CdMnS/CdS core/multi-shell nanoplatelets has shown that the interband emission acquires a net circular polarization of σ_+ (left circular polarization, LCP) in the presence of an externally applied magnetic field.[7] This has been attributed to the exchange interaction between the carrier spins and those of the Mn ions.[11] In contrast, the non-magnetic (CdSe/CdS) core/multi-shell structures exhibit σ_- (right circular polarization, RCP) net circular polarization when an external magnetic field is applied.[7] The photoluminescence (PL) spectrum is asymmetric and contains two distinct spectral features. This asymmetry has been previously observed in CdSe/CdZnS and CdSe/CdS nanoplatelets.[12] In this paper, we systematically study and discuss these spectral features as well as their temporal evolution and individual circular polarizations. Based on these results, a model for the recombination channels associated with each feature is also proposed.

Here, we present data from two sets of nanoplatelet heterostructures: (a) a magnetic sample, which is comprised of a CdSe core (5 monolayer (ML) in vertical thickness) surrounded by a $Cd_{0.985}Mn_{0.015}S$ shell (1 ML on every side) and finally an additional CdS shell (1 ML) and (b) a non-magnetic sample, which is comprised of the same CdSe core (5 ML) surrounded by only a CdS shell (1 ML) with no Mn doping. In these samples, one monolayer is approximately 0.3 nm thick, and the lateral core dimensions are 55 ± 6 nm $\times$ 10 ± 2 nm; the values for these dimensions were obtained using TEM.[7] Further details regarding these samples have been described by Delikanli *et al.* where the magnetic (non-magnetic) sample corresponds to sample 1 (3).[7]

The PL measurements were carried out by placing the samples in a variable-temperature, optical magnet cryostat. The magnetic field was applied along the direction perpendicular to the sample substrate, hereby referred to as the z-axis. The samples were excited using the linearly polarized 514.5 nm output of an argon-ion laser. The experiment was performed in the Faraday geometry in which the direction of the emitted light propagation is parallel to the applied magnetic field. The combination of a quarter-wave plate and a linear polarizer was placed in appropriate configurations before the spectrometer entrance slits to separate the LCP (σ_+) from the RCP (σ_-) components of the emission. The PL was spectrally analyzed by a single monochromator equipped with a charged coupled device (CCD). The time-resolved photoluminescence (trPL) was excited using a pulsed laser system with a repetition rate of 250 kHz and a pulse duration of <200 fs with a pulse energy density of 10 μJ/cm^2. The pulsed excitation was generated using an optical parametric amplifier tuned to 514 nm. The trPL was spectrally resolved using a monochromator and temporally analyzed by a streak camera with a temporal resolution of 60 ps.

a)Electronic mail: volkan@bilkent.edu.tr
b)Electronic mail: petrou@buffalo.edu

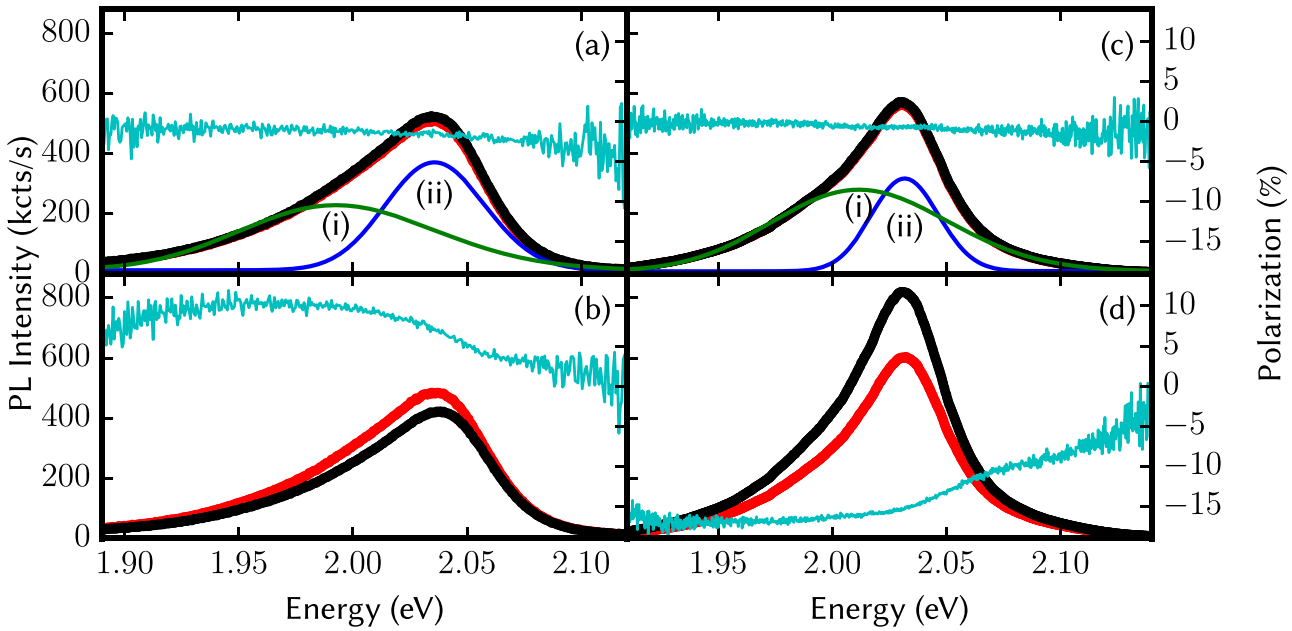

FIG. 1. PL spectra from the magnetic (a), (b) and non-magnetic (c), (d) samples using an excitation wavelength of 514 nm at a temperature of 7 K. The red (black) points indicate σ_+ (σ_-) circularly polarized PL components. The cyan line is the calculated circular polarization. In the upper panels (a), (c), the applied magnetic field is 0 T and in the lower panels (b), (d) it is 7 T. The green and blue lines in panels (a) and (c) are the result of a fitting that uses two Gaussian functions to the asymmetric PL spectra.

In Figures 1(a) and 1(b), we show the PL spectra from the magnetic sample at $B = 0$ T and $B = 7$ T; panels (c) and (d) depict those under the same conditions for the non-magnetic sample. The PL is analyzed as σ_+ (red) and σ_- (black). Also plotted is the degree of circular polarization P (cyan line) defined as $(I_+ - I_-)/(I_+ + I_-)$, where I_+ (I_-) is the intensity of the σ_+ (σ_-) PL component. The PL has an asymmetric shape for both samples and can be fit by the sum of two Gaussian functions with peaks at approximately 1.99 and 2.04 eV for the magnetic sample and 2.01 and 2.03 eV for the non-magnetic sample. These Gaussian functions are indicated by the green and blue lines marked (i) and (ii), respectively. The energy-polarization plot in panel (b) shows that the circular polarization has a maximum approximately coincident with feature (i). This strongly indicates that the recombination process associated with feature (i) involves carriers in the vicinity of Mn ions at the core/shell interfaces of the magnetic sample. The fact that the hole-Mn exchange interaction is several times stronger than the electron-Mn interaction[11] suggests that the localized carriers must be holes. The PL from the non-magnetic sample has a negative circular polarization in the presence of an applied magnetic field and exhibits no peak corresponding to either feature.

A superposition of the zero-field transmission and PL spectra is shown in Figure 2 for the magnetic sample. The strong absorption feature marked (ii) corresponds to PL feature (ii) shown in blue. In contrast, PL feature (i) in green does not have a corresponding absorption feature. Based on these results, we conclude that feature (ii) is excitonic, while feature (i) is not.[13] Absorption feature (iii) in Figure 2 has been attributed to interband transitions associated with light holes.[7] Similar results have been observed for the non-magnetic sample. In the inset of Fig. 2, we plot the intensity ratio I_{ii}/I_i of the PL features (ii) and (i), as a function of temperature for the magnetic sample. This ratio increases with increasing temperature, suggesting that recombination channel (i) involves holes that are localized and as the temperature increases, a smaller fraction of the photo-excited holes remains localized. The plot has two distinct regions: a low temperature region where T is between 10 K and 90 K and a high temperature region where T is between 90 K and 200 K. While the ratio is increasing, it does not significantly vary in the low-temperature range; however, in the high-temperature range, we observe a sharp monotonic increase. From the data of the inset, we can extract localization energies from each region using the relationship $\ln(I_{ii}/I_i) = -\Delta E/k_B T$.

A plot of $\ln(I_{ii}/I_i)$ versus $1/T$ is shown in Figure 3. The fit of the data in the low-temperature region has a very small slope, corresponding to a near-zero localization energy of 0.043 meV which suggests the presence of a band shown in the inset of Figure 3 in light blue. A possible origin of this

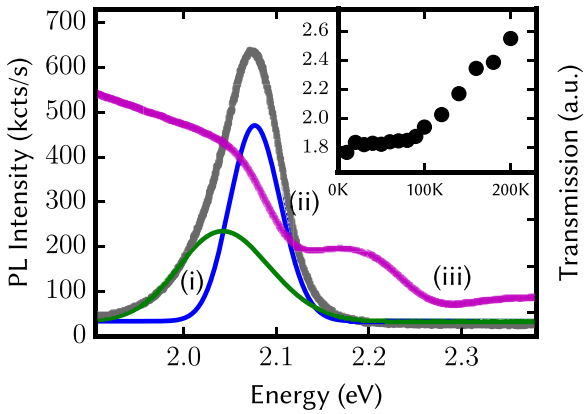

FIG. 2. Comparison of the zero-field PL (grey) and transmission spectra (magenta) for the magnetic sample. The blue (green) line is the result of a Gaussian fit to the high (low) energy component. The feature identified as (iii) is identified as a transition involving light holes. The inset shows the evolution of the ratio I_{ii}/I_i as a function of temperature.

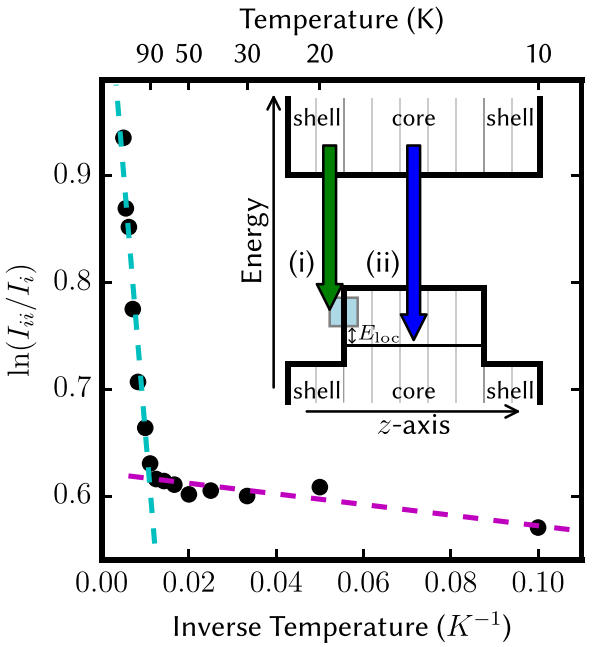

FIG. 3. The value of $\ln(I_{ii}/I_i)$ is plotted versus 1/T; here, I_i and I_{ii} represent the fitted PL peak intensities. Two temperature regions are identified, and linear fits to the high (low) temperature data are indicated by the cyan (magenta) dashed line. The inset is a diagram of the recombination scheme of our core/multi-shell nanoplatelet heterostructures. The vertical axis represents energy and the horizontal axis, the position along the z (vertical) dimension. The separation between light grey lines indicates the thickness of single monolayers. The two proposed recombination channels are indicated by the green and blue arrows marked (i) and (ii) and correspond to the PL features identified in Figure 1.

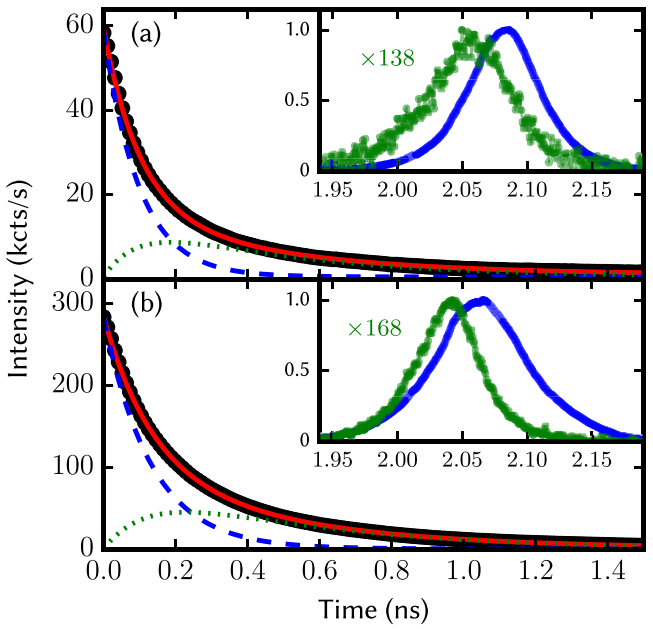

FIG. 4. The temporal evolution of the PL intensity from the magnetic sample is shown in panel (a) and that of the non-magnetic sample is shown in panel (b) using black points. The calculated intensities of features (i) and (ii) are shown using dotted green and dashed blue lines, respectively. The sum of these intensities is indicated by the red lines. The data of the insets represent time slices of the trPL spectra at $\Delta t = 0$ ns (blue points) and at $\Delta t = 3.5$ ns (green points). These inset spectra have been normalized and dark count-corrected so as to have the same peak intensity, and the green numbers indicate the magnification factor for the spectra at $\Delta t = 3.5$ ns.

band is the localized state energy-variation in the *xy*-plane of the nanoplatelet. In contrast, the high temperature region yields a localization energy of 4.2 meV. For this high-temperature region, thermal energy is now sufficient to delocalize holes from the interface defect state band to the bottom of the lowest heavy hole confinement state allowing recombination via channel (ii).

To determine the origin of the two PL features, we studied the recombination dynamics in our samples using trPL spectroscopy. For each time slice ($\delta t = 10$ ps), the spectrum is fit to a Gaussian function; examples of the time slices are given as insets in panels (a) and (b) of figure 4. for the magnetic and non-magnetic samples, respectively. In these insets, the vertical axis represents the normalized PL intensity and the horizontal energy. The spectra shown as insets correspond to time delays of 0 ns (blue points) and 3.5 ns (green points). We note that these time slices do not exhibit the same degree of asymmetry as the PL spectra. A rate equation-based model that was developed to describe the PL dynamics is given in the supplementary information.[14] The results of this analysis are summarized in Figures 4(a) and 4(b) for the magnetic (non-magnetic) sample as follows: calculated intensity of the PL feature (i) using dotted green lines; calculated intensity of the PL feature (ii) using dashed blue lines; calculated integrated PL intensity using red lines (sum of green and blue data); and the experimental PL intensity integrated over all wavelengths using black points. The lifetimes extracted from the rate equations, τ_f and τ_s (values summarized in the supplementary material) are discussed in terms of the following model.[14]

In this section, we discuss a proposed model that can explain our experimental observations. In the inset of Figure 3, we show a diagram of the recombination scheme for our samples. We attribute the PL features, (i) and (ii) to the corresponding interband transitions under the same label shown in the figure. Transition (ii) is excitonic in nature as indicated by the transmission spectra shown in Figure 2. Transition (i), on the other hand, does not have a signature in the absorption spectrum; in addition, for the magnetic sample, it is associated with a large degree of circular polarization in the presence of an applied magnetic field, indicating the participation of carriers in the vicinity of Mn ions which are located at the core/shell interfaces. Therefore, we attribute this feature to recombination of electrons with holes localized at defect states on the core/shell interfaces. This is shown by the *P* versus *E* plot for the magnetic sample shown in Figure 1(b) (cyan line) where the maximum of *P* (11%) occurs at the peak energy of feature (i); the circular polarization at the peak energy of feature (ii) on the other hand is only 4%. This evidence allows us to identify the position of the localized states involved in transition (i) at the core/shell interface using the hole-magnetic ion interaction as a marker.

The fast and slow timescales (τ_f and τ_s) obtained from the rate equation model are identified as closely related to the corresponding recombination times for channels (ii) and (i), respectively. The relaxation of holes to the defect states at the core/shell interface occurs much faster than either of these timescales.[15,16] The short time scale, τ_f, on the order of hundreds of picoseconds, is compatible with measurements of the lifetime from CdSe core-only nanoplatelets.[10]

According to Tessier *et al.*, measurements of core-crown CdSe/CdS NPLs exhibited a dramatic increase in the fluorescence lifetime when a CdS crown was grown (lateral extension).[12] This is in accordance with our observation of recombination involving holes localized in defect states at the core/shell interfaces (feature (i)). The stronger hole localization in our samples leads to a decreased electron-hole wave function overlap and thus a decreased oscillator strength and an increased lifetime.[17–20]

We have studied spectral characteristics of the two features of the emission spectra from both magnetic and non-magnetic core/multi-shell nanoplatelet heterostructures. While the high-energy feature has a strong absorption signature, the low-energy feature has no associated absorption. In the presence of a magnetic field, the non-magnetic nanoplatelets have a spectrally featureless, negative PL circular polarization. In contrast, the positive PL circular polarization exhibited by the magnetic sample is centered on the low-energy PL feature. The PL circular polarization from the magnetic sample is an indication of hole-Mn interaction and is used as a marker that determines the location of the hole states participating in recombination channel (i). The trPL spectra from both samples do not exhibit the pronounced asymmetry observed in the time-integrated spectra. A rate equation-based model is proposed which shows that the lower energy process (i) is significantly slower than the higher energy process (ii). This approach will be useful for the analysis of optical measurements in related colloidal nanoplatelets in the future.

The authors would like to thank EU-FP7 Nanophotonics4Energy NoE, and TUBITAK EEEAG 109E002, 109E004, 110E010, 110E217, and 112E183, and NRF-RF-2009-09, NRF-CRP-6-2010-02, and A*STAR of Singapore for the financial support. H.V.D. acknowledges support from ESF-EURYI and TUBA-GEBIP. Work at the University at Buffalo was supported by NSF DMR 1305770.

[1]J. H. Yu, X. Liu, K. E. Kweon, J. Joo, J. Park, K.-T. Ko, D. W. Lee, S. Shen, K. Tivakornsasithorn, J. S. Son, J.-H. Park, Y.-W. Kim, G. S. Hwang, M. Dobrowolska, J. K. Furdyna, and T. Hyeon, "Giant Zeeman splitting in nucleation-controlled doped CdSe:Mn^{2+} quantum nanoribbons," Nat. Mater. **9**(1), 47 (2010).

[2]R. Fainblat, J. Frohleiks, F. Muckel, J. H. Yu, J. Yang, T. Hyeon, and G. Bacher, "Quantum confinement-controlled exchange coupling in manganese(II)-doped CdSe two-dimensional quantum well nanoribbons," Nano Lett. **12**(10), 5311 (2012).

[3]S. Ithurria and D. V. Talapin, "Colloidal atomic layer deposition (c-ALD) using self-limiting reactions at nanocrystal surface coupled to phase transfer between polar and nonpolar media," J. Am. Chem. Soc. **134**(45), 18585 (2012).

[4]B. Mahler, B. Nadal, C. Bouet, G. Patriarche, and B. Dubertret, "Core/shell colloidal semiconductor nanoplatelets," J. Am. Chem. Soc. **134**(45), 18591 (2012).

[5]M. D. Tessier, P. Spinicelli, D. Dupont, G. Patriarche, S. Ithurria, and B. Dubertret, "Efficient exciton concentrators built from colloidal core/crown CdSe/CdS semiconductor nanoplatelets," Nano Lett. **14**(1), 207 (2014).

[6]S. Delikanli, B. Guzelturk, P. L. Hernandez-Martinez, T. Erdem, Y. Kelestemur, M. Olutas, M. Z. Akgul, and H. V. Demir, "Continuously tunable emission in inverted type-I CdS/CdSe core/crown semiconductor nanoplatelets," Adv. Funct. Mater. **25**(27), 4282 (2015).

[7]S. Delikanli, M. Z. Akgul, J. R. Murphy, B. Barman, Y. Tsai, T. Scrace, P. Zhang, B. Bozok, P. L. Hernandez-Martinez, J. Christodoulides, A. N. Cartwright, A. Petrou, and H. V. Demir, "Mn^{2+}-Doped CdSe/CdS core/multishell colloidal quantum wells enabling tunable carrier-dopant exchange interactions," ACS Nano **9**(12), 12473 (2015).

[8]Y. Kelestemur, M. Olutas, S. Delikanli, B. Guzelturk, M. Z. Akgul, and H. V. Demir, "Type-II colloidal quantum wells: CdSe/CdTe core/crown heteronanoplatelets," J. Phys. Chem. C **119**(4), 2177 (2015).

[9]V. A. Vlaskin, R. Beaulac, and D. R. Gamelin, "Dopant-carrier magnetic exchange coupling in colloidal inverted core/shell semiconductor nanocrystals," Nano Lett. **9**(12), 4376 (2009).

[10]S. Ithurria, M. D. Tessier, B. Mahler, R. P. S. M. Lobo, B. Dubertret, and A. L. Efros, "Colloidal nanoplatelets with two-dimensional electronic structure," Nat. Mater. **10**(12), 936 (2011).

[11]J. K. Furdyna, "Diluted magnetic semiconductors," J. Appl. Phys. **64**(4), R29 (1988).

[12]M. D. Tessier, B. Mahler, B. Nadal, H. Heuclin, S. Pedetti, and B. Dubertret, "Spectroscopy of colloidal semiconductor core/shell nanoplatelets with high quantum yield," Nano Lett. **13**(7), 3321 (2013).

[13]P. J. Pearah, J. Klem, C. K. Peng, T. Henderson, W. T. Masselink, H. Morkoç, and D. C. Reynolds, "Optical transitions and acceptor binding energies in GaAs/$Al_xGa_{1-x}As$ single quantum well heterostructures grown by molecular beam epitaxy," Appl. Phys. Lett. **47**(2), 166 (1985).

[14]See supplementary material at http://dx.doi.org/10.1063/1.4953840 for further description of this model.

[15]V. I. Klimov, P. Haring-Bolivar, H. Kurz, and V. A. Karavanskii, "Optical nonlinearities and carrier trapping dynamics in CdS and Cu_xS nanocrystals," Superlattices Microstruct. **20**(3), 395 (1996).

[16]V. Klimov, P. H. Bolivar, and H. Kurz, "Ultrafast carrier dynamics in semiconductor quantum dots," Phys. Rev. B. **53**(3), 1463 (1996).

[17]L. V. Kulik, V. D. Kulakovskii, M. Bayer, A. Forchel, N. A. Gippius, and S. G. Tikhodeev, "Dielectric enhancement of excitons in near-surface quantum wells," Phys. Rev. B **54**, R2335 (1996).

[18]E. A. Muljarov, S. G. Tikhodeev, N. A. Gippius, and T. Ishihara, "Excitons in self-organized semiconductor/insulator superlattices: PbI-based perovskite compounds," Phys. Rev. B **51**, 14370 (1995).

[19]T. Takagahara, "Effects of dielectric confinement and electron-hole exchange interaction on excitonic states in semiconductor quantum dots," Phys. Rev. B **47**, 4569 (1993).

[20]D. B. Tran Thoai, R. Zimmermann, M. Grundmann, and D. Bimberg, "Image charges in semiconductor quantum wells: Effect on exciton binding energy," Phys. Rev. B **42**, 5906 (1990).